Applied Acoustics 181 (2021) 108151

Contents lists available at ScienceDirect

Applied Acoustics

journal homepage: www.elsevier.com/locate/apacoust

Fault diagnosis of planetary gearbox based on acoustic signals

Jiachi Yao [a,b], Chao Liu [a,c,*], Keyu Song [a,b], Chenlong Feng [a,b], Dongxiang Jiang [a,b]

[a] Department of Energy and Power Engineering, Tsinghua University, Beijing 100084, China
[b] State Key Laboratory of Control and Simulation of Power System and Generation Equipment, Tsinghua University, Beijing 100084, China
[c] Key Laboratory of Thermal Science and Power Engineering of Ministry of Education, Tsinghua University, Beijing 100084, China

ARTICLE INFO

Article history:
Received 15 September 2020
Received in revised form 31 March 2021
Accepted 24 April 2021
Available online 14 May 2021

Keywords:
Planetary gearbox
Acoustic signals
Fault diagnosis
Fourier decomposition method
Feature extraction

ABSTRACT

The reliability of planetary gearbox is extremely important for safe and reliable operation. In this work, a fault diagnosis method based on acoustic signals is proposed for planetary gearbox, where the generated acoustic signals are nonlinear and non-stationary. First, the Fourier decomposition method (FDM) is utilized to decompose the measured acoustic signals into Fourier intrinsic band functions (FIBFs). Compared with the traditional empirical mode decomposition (EMD) method, FDM has better decomposition effect results without end effects and mode aliasing issues. Second, the comprehensive feature parameters of energy and TESK (time and envelope spectrum kurtosis) are adopted for overcoming the noisy and weak acoustic signals. Compared with a single feature parameter, the comprehensive feature parameters can significantly improve the accuracy of fault diagnosis. Third, the Random Forest (RF) classification algorithm is adopted for setting up the fault diagnosis method. Experimental results show that the fault diagnosis accuracy rate of the proposed FDM-based method using the acoustic signals reaches up to 96.32% under the limited sample data conditions, which achieved better fault diagnosis effect than vibration signals in the experimental conditions.

1. Introduction

With the development of modern large-scale production and the progress of science and technology, modern mechanical equipment is developing towards the direction of structural complexity and automation. The working intensity of mechanical equipment continues to increase, and the efficiency and automation degree are getting higher and higher. As the equipment is more complex and the components are more compact, a chain reaction will be erupted when a small failure occurs, causing catastrophic destruction of the entire equipment and even the equipment-related environment. The crash of the US space shuttle Columbia was a vicious accident that shocked the world due to a malfunction of a certain component. Therefore, it is urgent to conduct research on mechanical equipment condition monitoring and fault diagnosis technology. The planetary gearbox is widely applied and the key component of mechanical equipment such as wind turbines, reducer and motor. In addition, the operating conditions of the planetary gearbox are very critical, thus it is important to carry out condition monitoring and fault diagnosis of the planetary gearbox [1–5].

An effective condition monitoring and fault diagnosis technology needs to ensure the stable and continuous operation of planetary gearbox. By monitoring and diagnosing the state of the planetary gearbox, the normal, abnormal and early warning conditions of planetary gearbox can be obtained. Then the planetary gearbox can be repaired and maintained according to the various status information of the planetary gearbox. Therefore, the failure rate of the planetary gearbox could be reduced, the maintenance costs can be reduced, the reliability and safety can also be improved [6].

At present, the monitoring and diagnosis method is mostly based on vibration measurements (accelerations for gearbox) [7–12]. The vibration based fault diagnosis technology has many advantages, such as inexpensive accelerometer, easy access to vibration signals, containing rich information of the equipment status. However, there are also disadvantages for vibration-based methods. The accelerations are measured by contact measurement method, which limits the position of the installation. When the installation condition is poor, it will be difficult to install the sensor. In addition, in order to achieve better fault diagnosis effect, the vibration sensor needs to be installed as close to the monitored location. Otherwise, the measured vibrations will be seriously affected by interference noise in the system.

* Corresponding author at: Department of Energy and Power Engineering, Tsinghua University, Beijing 100084, China.
E-mail address: cliu5@tsinghua.edu.cn (C. Liu).

https://doi.org/10.1016/j.apacoust.2021.108151
0003-682X/

Recently, acoustic-based fault diagnosis techniques attract more and more attention [13–19]. Compared to the vibration-based fault diagnosis methods, there are few researches on acoustic-based fault diagnosis approaches. Acoustic signals of planetary gearbox are usually mixed with interference noise from other parts, such as reflected acoustic and overlapped acoustic. However, the acoustic-based fault diagnosis technology has many advantages. Acoustic signals are measured by non-contact measurement method, which is more convenient and immediate. In addition, the acoustic sensor is inexpensive and easy to access acoustic signals. The mechanical failures of planetary gearbox can be analyzed by acoustic signals.

In this context, this work focuses on planetary gearbox fault diagnosis method using acoustic signals. Acoustic signals are nonlinear and non-stationary signals. The EMD method is the most widely used method for processing nonlinear and non-stationary signals [20]. Researchers have proposed many fault diagnosis methods based on EMD [21–23]. Due to the EMD method has end effect and mode aliasing problems, therefore many researchers have proposed some improved EMD methods, such as EEMD method [24], FEEMD method [25], CEEMD method [26], ICEEMD method [27], etc. Unfortunately, these improved EMD method are computationally expensive. Besides, these EMD-based methods essentially lack rigorous mathematical derivation. Thus, researchers are looking for new signal decomposition methods. One of these methods is empirical wavelet method (EWT) [28]. Later, some researchers proposed enhanced EWT (EEWT) [29]. EWT and EEWT methods decompose mixed signals based on adaptive wavelet filter bank. But they need to know the number of modes in advance and cannot decompose the signals with overlapped spectra [28,29]. Another method is the variational mode decomposition (VMD) method [30]. As an alternative to EMD method, VMD method has a wide range of applications in the field of fault diagnosis [31–34]. However, the VMD method needs to determine the mode numbers in advance.

Different from the above methods, Fourier decomposition method (FDM) is free from parameter settings and has a rigorous mathematical theory [35]. Through the FDM method, the mixed signal can be decomposed into a small number of band-limited orthogonal functions which called Fourier intrinsic band functions (FIBFs). The FDM method is shown to be more suitable for analyzing nonlinear and non-stationary signals [36–38]. In this study, a new and efficient approach is proposed for planetary gearbox fault diagnosis using acoustic signals. The proposed method is called "FCRF", which is formed by combining the FDM, Comprehensive feature parameters and Random Forest. Firstly, the measured acoustic signals are decomposed into FIBFs through FDM. Then the comprehensive feature parameters of energy and TESK (time and envelope spectrum kurtosis) are extracted from each FIBF. Finally, the comprehensive feature parameters are passed to the Random Forest (RF) classifier to diagnose faults. Experimental data obtained from actual planetary gearbox was utilized to verify the effectiveness of the proposed FCRF method. Compared with the existing methods, the proposed FCRF method performs better.

The contributions of this work include: (Ⅰ) the acoustic sensor is utilized for monitoring and diagnosis of planetary gearbox; (Ⅱ) comprehensive feature parameters (energy and TESK) are required for acoustic sensor diagnosis, which is different from accelerometers; (III) the acoustic sensor has a better diagnostic effect than accelerometers under the experimental conditions of this work; (Ⅳ) a fault diagnosis method based on acoustic signals is proposed, which is called FCRF method.

The paper is organized as follows. In Section 2, the preliminaries of the Fourier decomposition method (FDM), acoustic signals feature extraction method and classification methods are described. In Section 3, the simulation results are applied for verifications and comparisons. Experimental results, comparison and discussions are studied in Section 4. Finally, the conclusions are summarized in Section 5.

2. Basic theory method

2.1. Fourier decomposition method (FDM)

The FDM algorithm, like the EMD algorithm, is an adaptive data-driven signal decomposition algorithm. But there are significant differences between the FDM method and the EMD method. The EMD algorithm essentially lacks a rigorous mathematical derivation process, and it has end effects and mode aliasing problems when decomposing mixed signals. As for FDM method, it has a rigorous mathematical derivation process. Besides, FDM method does not need to determine the parameters in advance such as stopping criterion, interpolation type, et al. Through the FDM method, the mixed signal can be decomposed into a series of individual components, which are called Fourier intrinsic band functions (FIBFs) [35]. According to the definition, it has the following equation.

$$x(t) = \sum_{i=1}^{M} y_i(t) + a_0 \tag{1}$$

where $x(t)$ is represented the mixed signal. $y_i(t)$ is represented the FIBF, and $y_i(t) \in C^{\infty}[a,b], 1 \le i \le M$. a_0 is represented the mean value of $x(t)$.

Suppose $x[n]$ is the discrete signal, the $x[n]$ can be written as follows by using the discrete Fourier transform (DFT).

$$x[n] = \sum_{K=0}^{N-1} X[k]\exp(j2\pi kn/N) \tag{2}$$

where N is the length of the signal.

The DFT of the signal $x[n]$ is

$$X[k] = (1/N)\sum_{n=0}^{N-1} x[n]\exp(-j2\pi kn/N) \tag{3}$$

For the even values of N,

$$\begin{aligned} x[n] = X[0] &+ \sum_{k=1}^{N/2-1} X[k]\exp(j2\pi kn/N) \\ &+ X[N/2]\exp(j\pi n) \\ &+ \sum_{k=N/2+1}^{N-1} X[k]\exp(j2\pi kn/N) \end{aligned} \tag{4}$$

For the odd values of N,

$$\begin{aligned} x[n] = X[0] &+ \sum_{k=1}^{(N-1)/2} X[k]\exp(j2\pi kn/N) \\ &+ \sum_{k=(N-1)/2+1}^{N-1} X[k]\exp(j2\pi kn/N) \end{aligned} \tag{5}$$

As the $x[n]$ is real, $z_1[n]$ is the complex conjugate of $z_2[n]$.

$$z_1[n] \triangleq \sum_{k=1}^{N/2-1} X[k]\exp(j2\pi kn/N) \tag{6}$$

$$z_2[n] \triangleq \sum_{k=N/2+1}^{N-1} X[k]\exp(j2\pi kn/N) \tag{7}$$

For even values of N, the following can be obtained.

$$x[n] = X[0] + 2\mathrm{Re}\{z_1[n]\} + X[N/2](-1)^n \tag{8}$$

For odd values of N, the following can be obtained.

$$x[n] = X[0] + 2\mathrm{Re}\{z_1[n]\} \tag{9}$$

Here, the analytic signal $z_1[n]$ can be written as

$$\sum_{k=1}^{N/2-1} X[k]\exp(j2\pi kn/N) = \sum_{i=1}^{M} a_i[n]\exp(j\varphi_i[n]) \tag{10}$$

where $a_i[n]$ is represented as the instantaneous phase (IP) of the ith analytical FIBF (AFIBF), $\varphi_i[n]$ is represented as the Instantaneous Amplitude (IA) of the ith AFIBF. M is the total number of AFIBFs.

For the forward search (low to high frequency scan, LTH-FS) of AFIBFs, it can be expressed as

$$a_i[n]\exp(j\varphi_i[n]) = \sum_{k=N_{i-1}+1}^{N_i} X[k]\exp(j2\pi kn/N) \tag{11}$$

where $N_0 = 0$, $N_M = (N/2-1)$.

The two conditions need to be met for the obtained AFIBFs.

$$\omega_i[n] = (\varphi_i[n+1] - \varphi_i[n-1])/2\pi \tag{12}$$

$$a_i[n] \geq 0 \tag{13}$$

For the backward search (high to low frequency scan, HTL-FS) of AFIBFs, it can be expressed as

$$a_i[n]\exp(j\varphi_i[n]) = \sum_{k=N_i}^{N_{i-1}-1} X[k]\exp(j2\pi kn/N) \tag{14}$$

2.2. Feature extraction method for acoustic signals

In this work, two feature parameters are utilized to extract information from acoustic signals. One is the energy [5], and the other is the time and envelope spectrum kurtosis (TESK) [39]. The acoustic signal is weaker than the vibration signal. In order to extract more fault information from the acoustic signal for fault diagnosis, it is necessary to study these two feature parameters in this work.

The energy of each component $x_i(t)$ can be calculated by

$$E_i = \int_{-\infty}^{+\infty} |x_i(t)|^2 dt, \quad i = 1,2,3,\cdots,n \tag{15}$$

Then the energy parameter can be obtained by

$$TE_i = E_i / \sum_{i=1}^{n} E_i, \quad i = 1,2,3,\cdots,n \tag{16}$$

The TESK parameter of each component is calculated by

$$TESK = \frac{E[x_i(t) - \mu_x]^4}{\sigma_x^4} \cdot \frac{E[es(f) - \mu_{ex}]^4}{\sigma_{es}^4} \tag{17}$$

where $x_i(t)$ is the decomposed components. $i = 1,2,3,\cdots,n$. μ_x is the mean value of $x_i(t)$. $\sigma_x$is the standard deviation of $x_i(t)$. $E(\cdot)$ is the expectation operation. $es(f)$ is the power spectrum of the envelope of $x_i(t)$. μ_{ex} is the mean value of $es(f)$. σ_{es} is the standard deviation of $es(f)$.

2.3. Classification method

After extracting the feature parameter information from the acoustic signal, the next step is to classify the faults based on the extracted feature parameter information. Firstly, the training samples are trained by classification model. Then the test samples are utilized to verify the classification effect. In order to compare the performance of different fault diagnosis classification methods, the following four classification methods are studied in this paper.

Back Propagation Neural Network (BPNN): BPNN consists of input layer, hidden layer and output layer. The performance of BPNN can be improved by adding hidden layers. BPNN has arbitrarily complex pattern classification capabilities and excellent multi-dimensional function mapping capabilities. In essence, the BPNN uses the square of the network error as the objective function and utilizes the gradient descent method to calculate the minimum value of the objective function [40].

Support Vector Machines (SVM): It is a classification model, which can be divided into hard interval support vector machine, soft interval support vector machine, nonlinear support vector machine. The SVM has many advantages. It can be mapped to high-dimensional space by using the kernel function. The nonlinear classification can be solved by using the kernel function. The SVM algorithm is sensitive to missing data, the choice of parameters and kernel functions [41].

Extreme Learning Machine (ELM): It is a type of machine learning system or method based on feedforward neural network. It suitable for supervised learning and unsupervised learning problems. The traditional ELM has a single hidden layer, and when compared with other shallow learning systems, such as single-layer perceptrons and support vector machine, it is considered to have advantages in terms of learning rate and generalization ability. Improved versions of ELM gain deep structure by adopting autoencoders to construct or stack hidden layers, which can perform characterization learning. The biggest characteristic of ELM is that for traditional neural networks, especially single hidden layer feedforward neural networks, it is faster than traditional learning algorithms under the premise of ensuring learning accuracy [42].

Random Forests (RF): In machine learning, the RF is a classifier containing multiple decision trees. It uses multiple trees to train and predict samples. The RF method has many advantages. It can produce highly accurate classifiers. It can handle a large number of input variables. It can assess the importance of variables when determining categories. When constructing the forest, it can produce an unbiased estimate of the generalized error internally. The learning process is very fast [43].

The four classification methods of BPNN, SVM, ELM and RF are utilized for planetary gearbox fault diagnosis based on acoustic signals feature parameter information, and the classification results are further researched in the following sections.

2.4. Flowchart of the proposed method

The flowchart of the proposed FCRF method for fault diagnosis of planetary gearbox based on acoustic signals is described in Fig. 1.

The procedure of the proposed method is as follows.

The acoustic sensor is utilized to measure the acoustic signals of planetary gearbox.
The FDM method is adopted to decompose the measured acoustic signals into several FIBFs. In order to remove the interference noise and improve the calculation efficiency, the six FIBF components with the largest correlation coefficient are selected for further analysis by the correlation coefficient method.
For the selected FIBF components, the comprehensive feature parameters of energy and TESK are calculated for each component.
The fault classification methods such as BPNN, SVM, ELM and RF are adopted to identify the planetary gearbox faults. Thus the fault diagnosis method of planetary gearbox based on acoustic signals can be obtained.

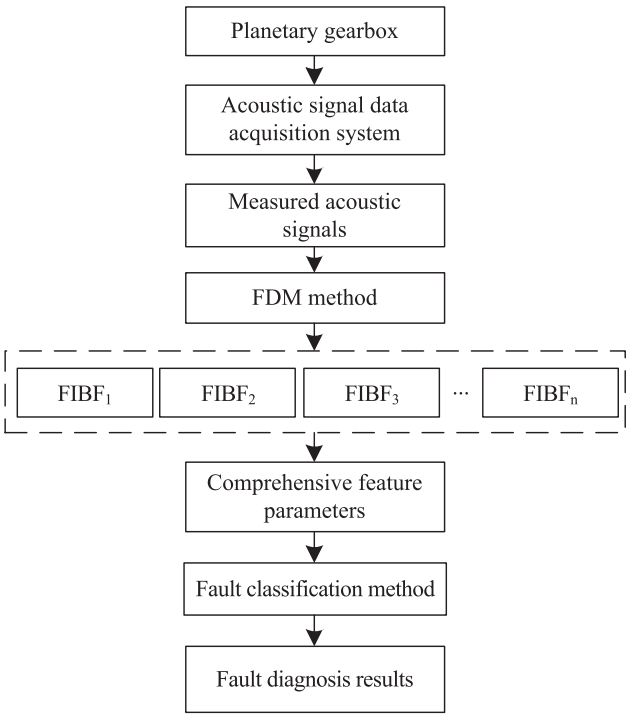

Fig. 1. Block diagram of the proposed method.

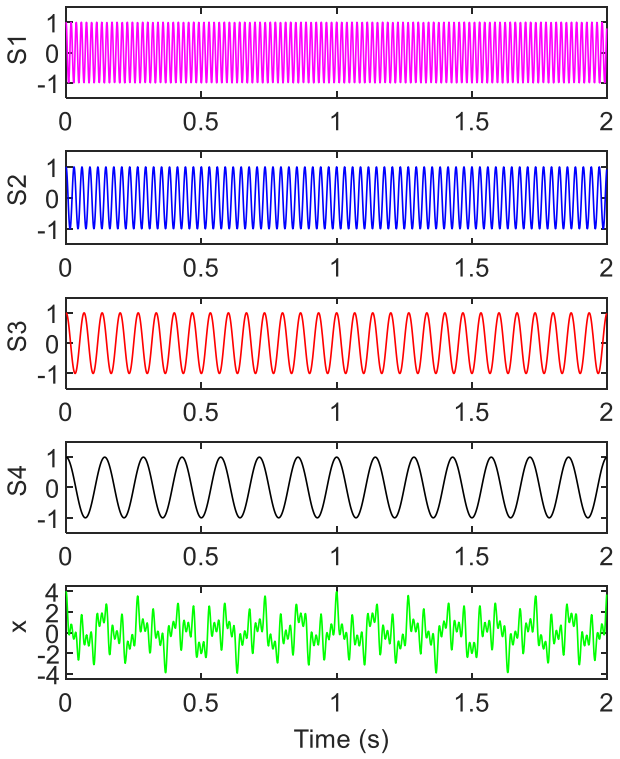

Fig. 2. The original signals.

3. Verification and comparisons using simulation results

Herein, simulated signals are generated to evaluate the performance of FDM algorithm. Considering that the frequency components generated by the planetary gearbox are low, thus four low-frequency harmonic signals are selected and the mixed signal $x(t)$ is shown as follows.

$$\begin{aligned} x(t) &= S1 + S2 + S3 + S4 + N \\ S1 &= \cos(2\pi \cdot 53 \cdot t) \\ S2 &= \cos(2\pi \cdot 34 \cdot t) \\ S3 &= \cos(2\pi \cdot 15 \cdot t) \\ S4 &= \cos(2\pi \cdot 7 \cdot t) \end{aligned} \tag{18}$$

where $\boldsymbol{t}$ is the time of the simulated signal, $\boldsymbol{N}$ represents the additive white Gaussian noise.

In the simulation test, the additive white Gaussian noise matrix $\boldsymbol{N}$ with a signal-to-noise-ration (SNR) of 80 dB was employed. The sampling frequency is 1024 Hz. The original signals are shown in Fig. 2.

Then the FDM method and EMD method are respectively carried out to decompose the mixed signal, and the decomposition results are shown in Fig. 3.

From the decomposition results calculated by EMD method and FDM method shown in Fig. 3, it is obvious that the decomposition performance of FDM is better. In Fig. 3(a), the decomposed signal S1 is different from the original signal S1, and this may be caused by mode aliasing problem. Besides, due to end effect issues, the decomposed signal S4 is different from the original signal S4, and it can be seen in the red rectangular box in Fig. 3(a).

In order to quantitatively compare the decomposition performance of the EMD method and FDM method, the following index [12] is utilized to compare the match degree between the decomposed signal and the original signal.

$$Index = -20 * \log10(\frac{\| y_i - x_i \|}{\| x_i \|}) \tag{19}$$

where, $i = 1, 2, 3, 4$. y_i is the decomposed signal. x_i is the original signal.

According to Equation (19), the larger the index is, the better extraction quality is. The calculation results under SNR 80 dB are shown in Table 1.

From Table 1, the scores of decomposed signals by FDM method are 27.44 dB, 27.10 dB, 34.15 dB and 37.24 dB, respectively. The scores of decomposed signals by EDM method are 7.47 dB, 13.93 dB, 13.65 dB and 1.43 dB. For S1 and S4, the EMD method scored only 7.47 dB and 1.43 dB, and they can also be seen from Fig. 3 that the decomposition results are not good. In general, the average scores of FMD method is 31.48 dB, which is higher than the EMD method scored 9.12 dB. Thus, it can be verified that the FDM method has better decomposition effect than EMD method.

In the real acoustic signals of planetary gearbox, there might be more types of interference noise in terms of the SNR. Thus, the simulated signal under low SNR is studied. Here, the SNR is decreased to 35 dB. The spectrogram of the mixed signal is shown in Fig. 4.

From Fig. 4(a), the mixed signal under SNR 80 dB contains less noise, while the mixed signal under SNR 35 dB contains more noise in Fig. 4(b). In a harsher condition, the decomposition results of FDM method and EMD method are shown in Fig. 5.

From Fig. 5, when the SNR is decreased to 35 dB, the decomposition effect of the EMD method is decreased. As shown in the red ellipse in Fig. 5(a), the S1 and S2 signals have seriously mode aliasing problems. But the FDM method still achieved a good decomposition effect. The quantitative index calculation results are shown in Table 2.

From Table 2, it can be seen that the EMD method scored 4.37 dB, 3.56 dB, 10.72 dB and 1.70 dB, and the average score is only 5.09 dB. But for FDM method, the average score is 30.60 dB, which is much higher than EMD method. For the S4, the calculation results of EMD under 80 dB is 1.43 dB, but the calculation results of EMD under 35 dB is 1.70 dB. This reason may be because the EMD algorithm can be regarded as a binary filter, which has a good

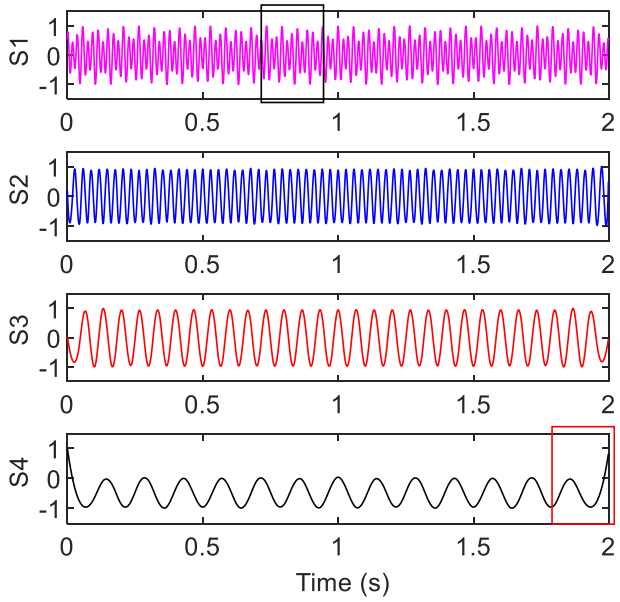

(a) EMD method

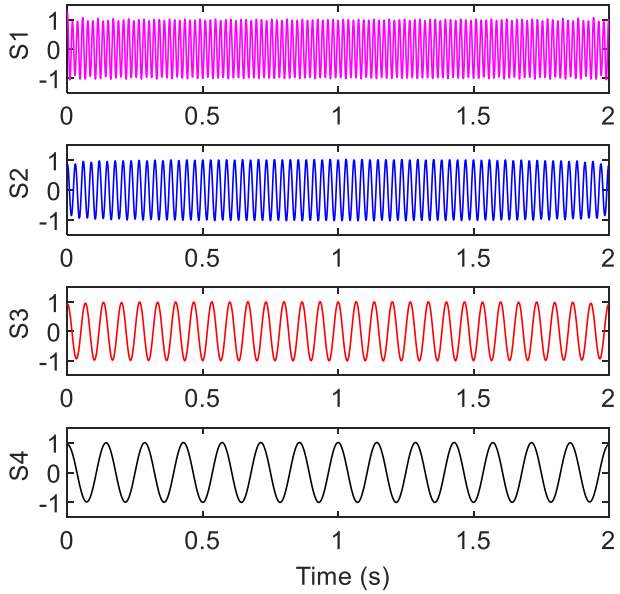

(b) FDM method

Fig. 3. The decomposition results under SNR 80 dB.

Table 1
The calculation results under SNR 80 dB (see Figs. 2 and 3).

Original source	Quantitative index (dB)	
	FDM	EMD
S1	27.44	7.47
S2	27.10	13.93
S3	34.15	13.65
S4	37.24	1.43
Average	31.48	9.12

decomposing effect on low frequency components. Thus the calculation results of EMD under different noise interference situations are almost the same for S4. But for S1, S2 and S3, the greater the interference noise, the lower the decomposition effect.

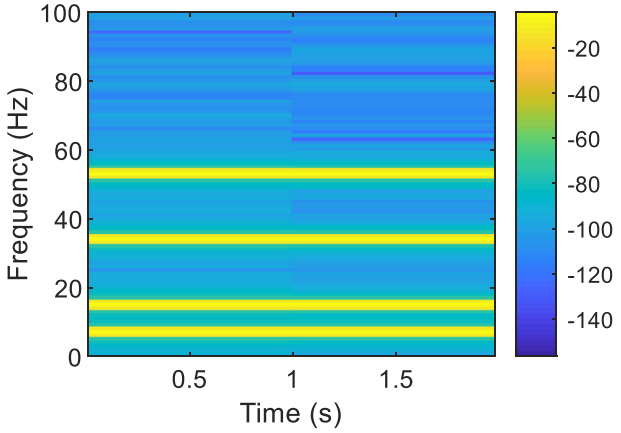

(a) The mixed signal under SNR 80 dB

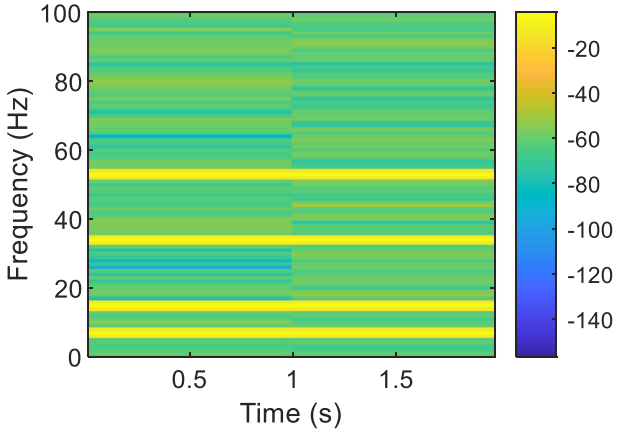

(b) The mixed signal under SNR 35 dB

Fig. 4. The spectrogram of the simulated signal.

In general, in a hasher condition and the SNR is only 35 dB, the FDM method still has excellent decomposition effect. FDM method has better performance than EMD method. Thus, in this paper, the FDM method is adopted to analyze acoustic signals for planetary gearbox fault diagnosis.

4. Experimental results and discussions

4.1. Experimental procedure

The entire test system is mainly included sound pressure sensor, accelerometer, charge amplifier, NI data acquisition card, NI acquisition chassis, data transmission line and computer. The sensitivity level of the sound pressure sensor is −25.8 dB (0 dB = 1V/Pa, at 1kHz) and the sensitivity of the accelerometer is 500 mV/g. The sampling frequency is 25.6 kHz. In the experiment, the fault diagnosis method based on acoustic signals is mainly researched. In addition, in order to further compare and analyze the results based on acoustic signals and vibration signals, an acceleration sensor is installed in the test bench.

The planetary gearbox in this work is used in actual transportation machinery, with tires wrapped around it, which makes it inconvenient to install the accelerometer directly on the planetary gearbox. Moreover, in some practical engineering applications, accelerometer is inconvenient to use in some situations such as high temperature, high corrosion, or the accelerometer cannot be installed when the mechanical equipment is running and the

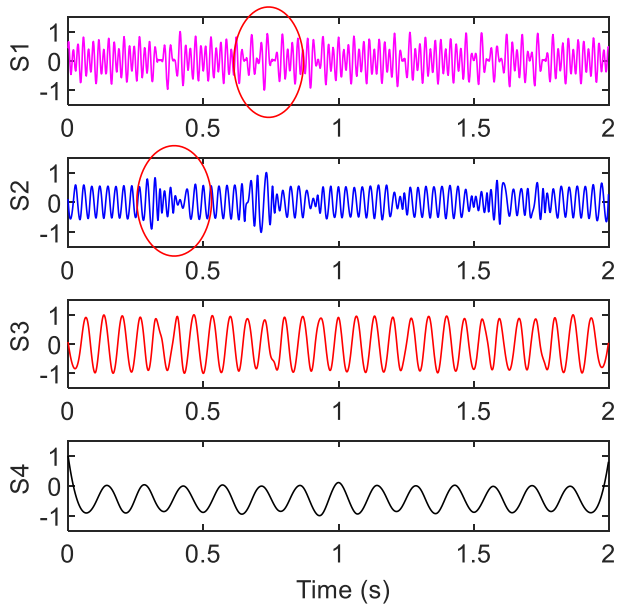

(a) EMD method

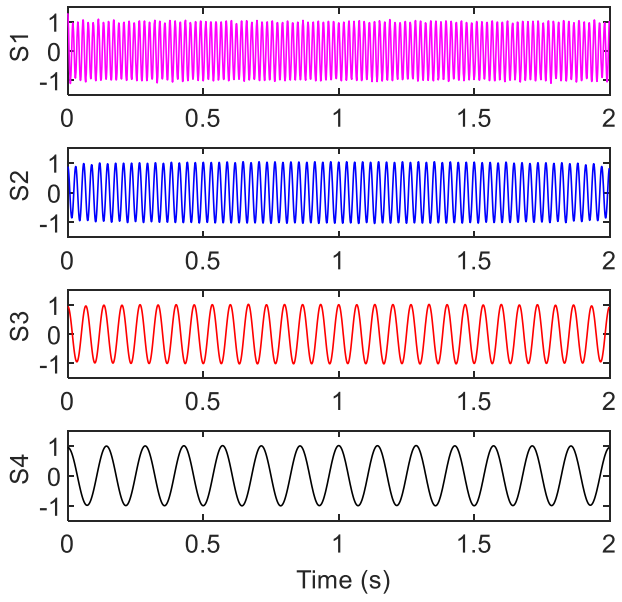

(b) FDM method

Fig. 5. The decomposition results under SNR 35 dB.

Table 2
The calculation results under SNR 35 dB (see Figs. 2 and 5).

Original source	Quantitative index (dB)	
	FDM	EMD
S1	25.25	4.37
S2	27.04	3.56
S3	34.05	10.72
S4	36.05	1.70
Average	30.60	5.09

structure of the installation site is limited. In order to solve the problem of fault diagnosis of planetary gearbox, a fault diagnosis technology based on acoustic signal is proposed. The advantages of acoustic-based fault diagnosis technology include non-contact measurement, simple equipment, fast speed, easy to measure acoustic signal, and no need to paste the sensor in advance. When measuring vibration signals, the accelerometer needs to be pasted on the surface of the mechanical structure, which is a contact measurement method. The measurement of the acoustic signal uses a non-contact measurement method, thus it is more convenient. However, the measured acoustic signals are usually easy to be disturbed by surrounding noise. In order to solve this problem, the measuring position of the sound pressure sensor is 1 cm away from the three-stage planetary gearbox in the test. Moreover, the measured sound pressure signals are preprocessed such as detrending item and de-averaging to eliminate the influence of other interference noise.

In the test, the vibration sensor can only be installed on the test bench and is relatively far away from the planetary gearbox. The installation positions of the acoustic signal sensor and vibration sensor are shown in Fig. 6.

In the actual operations, teeth failure is often occurred. In this experiment, four different conditions were tested, including (a) normal condition, (b) severe wearing of the inner gear ring, (c) four teeth loss in the inner gear ring, (d) two teeth loss in the inner gear ring. The rotating speed of the planetary gearbox was 300 rpm.

Considering that the planetary gearbox produces low-frequency components under working conditions, in order to improve calculation efficiency, the acoustic signals are down-sampling to 1024 Hz. For this three-stage planetary gearbox, the transmission ratio is 79. When the speed of the input shaft is 300 rpm, the speed of the output shaft is about 3.7975 rpm. In order to select the experimental data of one working cycle of the planetary gearbox, thus the 16-second data is intercepted for analysis in this work. For the sound pressure signal measured over a period of time, the 68 groups of 16-second experimental data is intercepted for subsequent analysis. Through tests, the time domain and frequency spectrum of the acoustic signal of a working cycle of the planetary gearbox are shown in Fig. 7.

From Fig. 7(a), S1 signal corresponds to normal condition. S2 signal corresponds to severe wearing of the inner gear ring condition. S3 signal corresponds to four teeth loss of the inner gear ring condition. S4 signal corresponds to two teeth loss of the inner gear ring condition. The time-domain waveform amplitude of S3 and S4 signals are slightly larger than S1 and S2 signals. This is because the S3 and S4 signals are tooth-loss faults, and they have a greater degree of failure. From Fig. 7(b), the frequency spectrum of S2 signal is significantly reduced at around 96 Hz. The frequency spectrum of S1, S3 and S4 signals is slightly different, but the difference is not obvious. It is almost impossible to diagnose faults only from the time domain and frequency spectrum of the acoustic signals. Therefore, it is necessary to employ advanced signal analysis methods to process the measured acoustic signals.

4.2. Calculation method and process

It is difficult to diagnose faults directly from the time domain and frequency spectrum of the acoustic signals. Therefore, it is necessary to adopt advanced signal processing methods to process and analyze the acoustic signals.

For the measured acoustic signals, firstly, the FDM method is utilized to decompose the acoustic signal into many FIBF components. Considering that the measured acoustic signals contain other interference noise, thus there is no need to analyze all the FIBF components. Here, according to the correlation coefficient method, the six FIBF components which have larger correlation coefficient with the acoustic signal are selected for subsequent calculations. The selected six FIBF components are shown in Fig. 8. The unit of the y-axis in Fig. 8 is V.

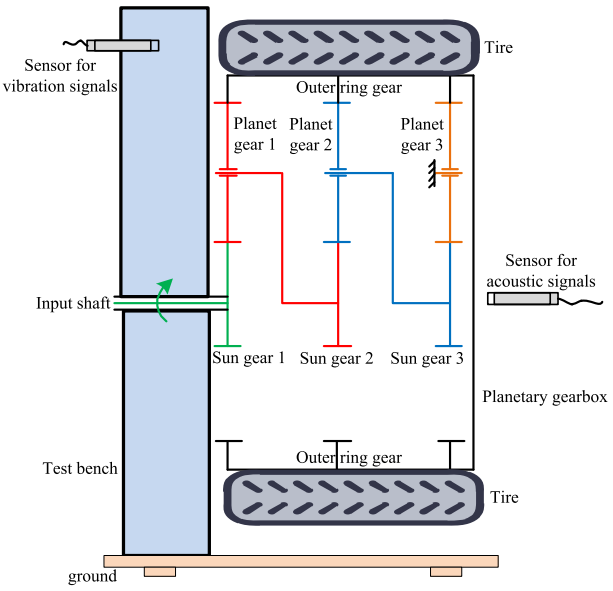

(a) Schematic diagram

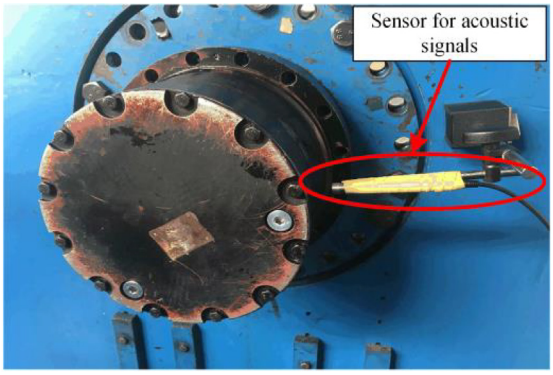

(b) Sound pressure measuring point

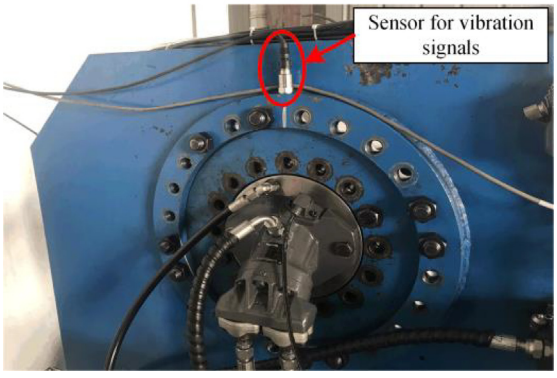

(c) Vibration measuring point

Fig. 6. Test setup.

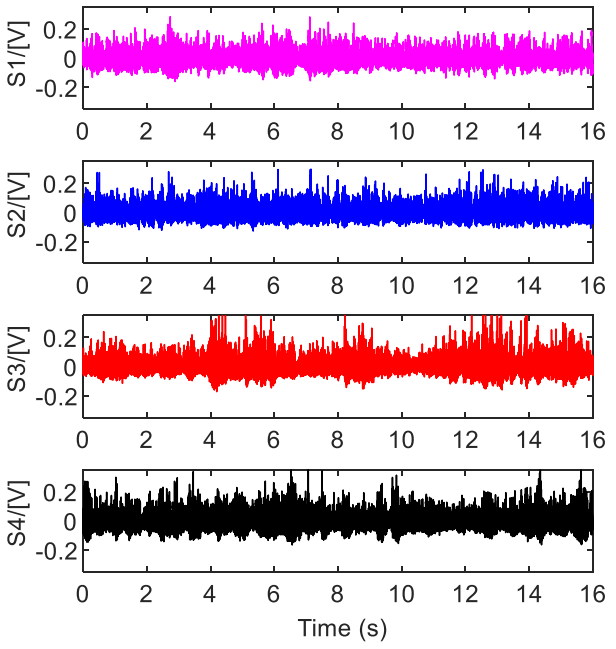

(a) The time domain

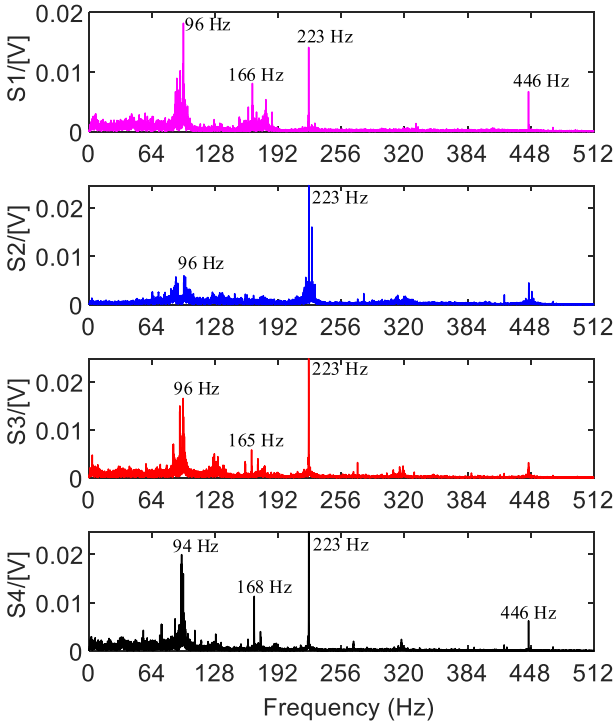

(b) The frequency spectrum

Fig. 7. The time domain and frequency spectrum.

Then the energy and TESK feature parameters are extracted for each FIBF component. The calculation results are shown in Table 3.

In order to compare the performance with other methods, the EMD method and EEMD method are employed to decompose the measured acoustic signals, respectively. Then the energy and TESK feature parameters are also calculated. The calculation results are shown in Tables 4 and 5.

From Tables 3–5, the energy and TESK feature parameters are obtained by FDM, EMD and EEMD method. The feature parameters of each component obtained by calculation have certain differences. Through the classification algorithm model, the nonlinear mapping relationship from the feature parameters to the fault diagnosis can be constructed based on the difference of the feature parameters of each component. Therefore, the planetary gearbox faults can be recognized. Fig. 9 is a histogram of the feature parameters of normalized energy and TESK by FDM method.

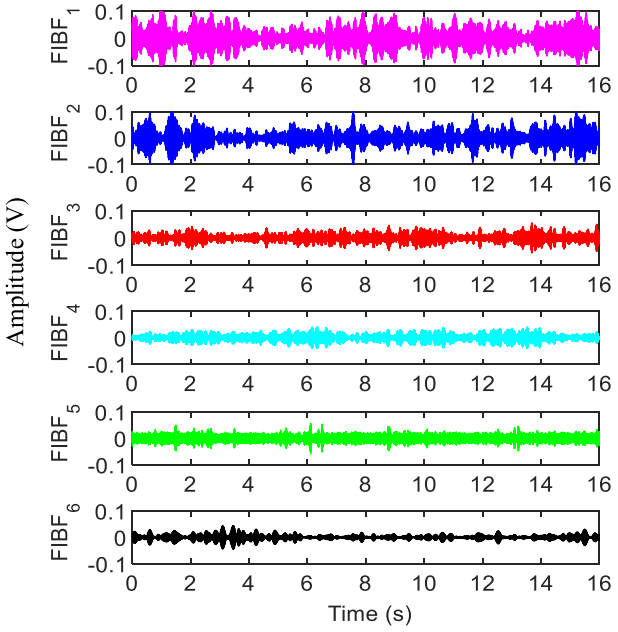

Fig. 8. The selected six FIBF components.

Table 3
The energy and TESK feature parameters calculated by FDM method.

Status	FIBFs	Energy feature	TESK feature
Normal condition	1	0.4473	0.1520
	2	0.3037	0.1738
	3	0.0796	0.1580
	4	0.0686	0.1453
	5	0.0654	0.1570
	6	0.0355	0.2139
Severe wear fault	1	0.5144	0.1477
	2	0.2166	0.1520
	3	0.1474	0.1655
	4	0.0541	0.1911
	5	0.0340	0.1781
	6	0.0334	0.1657
Four teeth loss fault	1	0.4573	0.1555
	2	0.2842	0.1578
	3	0.1156	0.1826
	4	0.0944	0.1692
	5	0.0272	0.1642
	6	0.0213	0.1706
Two teeth loss fault	1	0.6708	0.1712
	2	0.1765	0.1375
	3	0.0461	0.1564
	4	0.0403	0.1677
	5	0.0354	0.1769
	6	0.0310	0.1903

Table 4
The energy and TESK feature parameters calculated by EMD method.

Status	IMFs	Energy feature	TESK feature
Normal condition	1	0.4279	0.1420
	2	0.3743	0.2453
	3	0.1160	0.1565
	4	0.0386	0.1718
	5	0.0207	0.1381
	6	0.0226	0.1463
Severe wear fault	1	0.4835	0.1474
	2	0.3879	0.1596
	3	0.1003	0.1825
	4	0.0166	0.1621
	5	0.0073	0.1864
	6	0.0044	0.1620
Four teeth loss fault	1	0.5257	0.1581
	2	0.3356	0.1551
	3	0.0763	0.2114
	4	0.0270	0.1563
	5	0.0193	0.1612
	6	0.0159	0.1579
Two teeth loss fault	1	0.5436	0.1353
	2	0.3091	0.2517
	3	0.0833	0.1649
	4	0.0348	0.1541
	5	0.0176	0.1599
	6	0.0116	0.1342

Table 5
The energy and TESK feature parameters calculated by EEMD method.

Status	IMFs	Energy feature	TESK feature
Normal condition	1	0.4421	0.1419
	2	0.3779	0.2402
	3	0.1095	0.1613
	4	0.0347	0.1858
	5	0.0190	0.1352
	6	0.0168	0.1356
Severe wear fault	1	0.4933	0.1492
	2	0.3884	0.1613
	3	0.0945	0.1852
	4	0.0154	0.1696
	5	0.0062	0.1899
	6	0.0022	0.1448
Four teeth loss fault	1	0.5338	0.1577
	2	0.3394	0.1531
	3	0.0717	0.2138
	4	0.0256	0.1630
	5	0.0122	0.1643
	6	0.0172	0.1482
Two teeth loss fault	1	0.5589	0.1404
	2	0.3048	0.2339
	3	0.0806	0.1642
	4	0.0321	0.1539
	5	0.0150	0.1616
	6	0.0086	0.1459

From Fig. 9, it can be seen that the energy feature parameters of each component have significant differences. The TESK feature parameters have small differences. This is because the calculation formulas of the feature parameters are different, which leads to different information extracted from each component.

4.3. Fault diagnosis results and analysis

Through experiment, a total of 68 groups of sample data were obtained. Divide these experimental data into two parts, each with 34 groups of sample data. One part is used as the training set to train the model, and the other part is utilized as the test data to verify the effect. The classification methods such as BPNN, SVM, ELM and RF are utilized for fault diagnosis. The overall calculation results for planetary gearbox fault diagnosis are shown in Table 6.

From Table 6, it can be seen that the combined FDM with RF method has the accuracy of 96.32%. However, the EEMD-RF method and EMD-RF method have the accuracy of 94.12% and 92.65%, respectively. If the accuracy rate reaches 95%, it is considered to achieve excellent performance. Thus, it can be considered that the proposed FDM-RF method has the best performance.

For FDM-based method, by comparing with other classification algorithms, it can be seen that the BPNN and SVM have the accuracy of 58.09% and 51.47%, respectively. Their classification effect is not good. The classification effect of the SVM classifier is related to the selection of the kernel function and the amount of sample data. In this work, the kernel function of the SVM classifier is selected as the RBF function and the sample data is small, thus

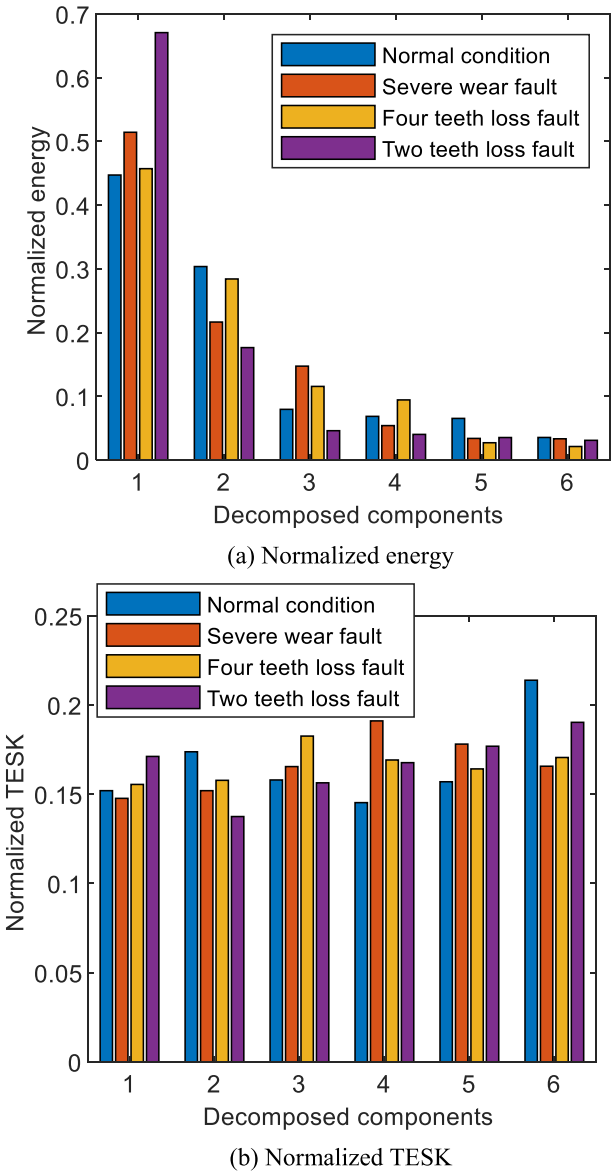

Fig. 9. Feature parameters of normalized energy and TESK by FDM method.

the classification effect of the SVM classifier is not good. The ELM has the accuracy of 90.44%. But for the RF, the fault diagnosis accuracy rate is as high as 96.32%. Therefore, RF is shown to be applicable in this case.

In the fault classification algorithm, the comprehensive feature parameters of energy and TESK are selected. In order to explore the influence of a single feature parameter on the fault classification effect, the fault diagnosis results based on a single feature parameter is calculated, and the calculation results are shown in Table 7.

From Table 7, it can be seen that when using the energy feature parameter, the accuracy of the FDM-RF method is 88.97%. As for TESK feature parameter, the accuracy of the FDM-RF method is 63.24%. It can be seen that the energy feature parameter has a better effect than the TESK feature parameter. It also can be seen for Fig. 9, the energy feature parameter of each component presents more variations than TESK feature parameter, and this could be learned by the classification algorithm for better performance. Therefore, the energy feature parameter has a better effect. Moreover, through adopting comprehensive feature parameters of energy and TESK, the effect of fault diagnosis is significantly improved, and the accuracy of FDM-RF method is up to 96.32%.

As reported in [5,39], for vibration signals, only using the energy or TESK can achieve good fault diagnosis results. However, the acoustic signals do not follow the above case. The possible reason is that the acoustic signals contain more types of interference noise than vibration signals, and the fault features in the acoustic signals are not as sensitive as that in the vibration signals. By using the comprehensive feature parameters of energy and TESK, the best performance is achieved using the proposed FCRF method based on acoustic signals in this work.

4.4. Comparison with vibration signals calculation results

In the experiment, the installation position of the vibration signal is shown in Fig. 6. For the measured vibration signals, the results with the proposed FCRF method are shown in Table 8.

From Table 8, it can be seen that the fault diagnosis accuracy of vibration signals is 93.38%, which is lower than the calculation results of the acoustic signals. Since the vibration sensor is installed relatively far away from the planetary gearbox, the fault features of the planetary gearbox are attenuated after transmitting through the complex path. Therefore, the vibration signals mea-

Table 8
Comparison of calculation results of vibration signals and acoustic signals.

Signals	Feature extraction	FCRF method
Vibration signals	Energy + TESK	93.38%
Acoustic signals	Energy + TESK	96.32%

Table 6
The overall calculation results for planetary gearbox fault diagnosis.

Decomposition method	Feature extraction	Detection rate (%)			
		BPNN	SVM	ELM	RF
FDM	Energy + TESK	58.09	51.47	90.44	**96.32**
EEMD	Energy + TESK	57.35	82.35	89.71	94.12
EMD	Energy + TESK	51.47	85.29	87.50	92.65

Table 7
The planetary gearbox fault diagnosis results based on different feature parameters.

Decomposition method	Feature extraction	Detection rate (%)			
		BPNN	SVM	ELM	RF
FDM	Energy	53.68	45.59	87.50	**88.97**
	TESK	41.18	55.15	63.97	**63.24**
	Energy + TESK	58.09	51.47	90.44	**96.32**

sured by the vibration sensor contain many other interference signals, which affect the classification performance. This also shows that the acoustic signals are more sensitive in this case, especially when the acceleration sensors are not able to be installed next to the monitored equipment.

5. Conclusions

In this work, the acoustic sensor is utilized for monitoring and diagnosis the planetary gearbox. Compared with the vibration signals, the real acoustic signals of planetary gearbox are smaller and are easy affected by the interference noise of surrounding environment. Thus it is challenging to diagnose planetary gearbox faults based on acoustic signals. To overcome this difficulty, an acoustic fault diagnosis method is proposed, which is called FCRF method.

For the real acoustic signals, the FDM method is utilized to decompose it into several FIBF components. In order to extract more information from the acoustic signals, the comprehensive feature parameters of energy and TESK are adopted. The extracted feature parameters are passed into the RF classification algorithm, one part is used for training, and the other part is employed to verify the classification effect. Compared with EMD and EEMD algorithms, FDM algorithm can achieve better effect even in a harsher condition with low SNR. In addition, compared with a single feature parameter, the comprehensive feature parameter (combined energy with TESK) can achieve better fault classification results. This is because the acoustic signals are relatively weak and contain more interference noise. Therefore, in order to obtain a better fault diagnosis effect, more information needs to be extracted and mined from the acoustic signals.

In this work, the training sample is limited for the RF model, but its accuracy rate is still up to 96.32% for the verification sample. The next step is to increase the acoustic signals sample library, and the fault diagnosis accuracy rate can be further improved.

In this work, the noise and vibration test research are carried out on a group of planetary gearboxes that failed in actual engineering applications, which has very important practical engineering application value. When a fault in the planetary gearbox causes a change in sound pressure signal, the proposed acoustic-based fault diagnosis technology can be used for diagnosis. The specific types that can be used for acoustic fault diagnosis are the tooth root crack, tooth surface pitting, tooth surface wear and other faults. Furthermore, when the planetary gearbox has a compound fault, it is necessary to further explore the applicability of the proposed acoustic-based fault diagnosis technology.

CRediT authorship contribution statement

Jiachi Yao: Conceptualization, Methodology, Software, Formal analysis, Validation, Investigation, Writing - original draft, Writing - review & editing. **Chao Liu:** Formal analysis, Supervision, Project administration, Writing - review & editing. **Keyu Song:** Data curation, Software, Methodology. **Chenlong Feng:** Investigation, Writing - review & editing. **Dongxiang Jiang:** Supervision, Project administration, Funding acquisition.

Declaration of Competing Interest

The authors declare that they have no known competing financial interests or personal relationships that could have appeared to influence the work reported in this paper.

Acknowledgment

This work was supported by the National Key R&D Program of China (Grant No. 2019YFF0216104), National Natural Science Foundation of China (Grant No. 11802152).

References

[1] Yun K, Tianyang W, Fulei C. Meshing frequency modulation assisted empirical wavelet transform for fault diagnosis of wind turbine planetary ring gear. Renew Energ 2019;132:1373–88. https://doi.org/10.1016/j.renene.2018.09.027.
[2] Cheng Z, Gao M, Liang X, Liu L. Incipient fault detection for the planetary gearbox in rotorcraft based on a statistical metric of the analog tachometer signal. Measurement 2020;151:107069. https://doi.org/10.1016/j.measurement.2019.107069.
[3] Salameh JP, Cauet S, Etien E, Sakout A, Rambault L. Gearbox condition monitoring in wind turbines: a review. Mech Syst Signal Pr 2018;111:251–64. https://doi.org/10.1016/j.ymssp.2018.03.052.
[4] Qin Y, Wang X, Zou JQ. The optimized deep belief networks with improved logistic sigmoid units and their application in fault diagnosis for planetary gearboxes of wind turbines. IEEE Trans Ind Electron 2019;66(5):3814–24. https://doi.org/10.1109/TIE.2018.2856205.
[5] Chen X, Yang Y, Cui Z, Shen J. Vibration fault diagnosis of wind turbines based on variational mode decomposition and energy entropy. Energy 2019;174:1100–9. https://doi.org/10.1016/j.energy.2019.03.057.
[6] Bangalore P, Patriksson M. Analysis of SCADA data for early fault detection, with application to the maintenance management of wind turbines. Renew Energ 2017;115:521–32. https://doi.org/10.1016/j.renene.2017.08.073.
[7] Wang TY, Han QK, Chu FL, et al. Vibration based condition monitoring and fault diagnosis of wind turbines planetary gearbox: a review. Mech Syst Signal Pr 2019;126:662–85. https://doi.org/10.1016/j.ymssp.2019.02.051.
[8] Koukoura S, Carroll J, Mcdonald A, et al. Comparison of wind turbines gearbox vibration analysis algorithms based on feature extraction and classification. IET Renew Power Gen 2019;13(14):2549–57. https://doi.org/10.1049/iet-rpg.2018.5313.
[9] Zhang J, Hu NQ. Fault diagnosis of sun gear based on continuous vibration separation and minimum entropy deconvolution. Measurement 2019;141:332–44. https://doi.org/10.1016/j.measurement.2019.04.049.
[10] Kong Y, Wang T, Chu F. Meshing frequency modulation assisted empirical wavelet transform for fault diagnosis of wind turbine planetary ring gear. Renew Energ 2019;132:1373–88. https://doi.org/10.1016/j.renene.2018.09.027.
[11] Qin Yi, Mao Y, Tang B, Wang Yi, Chen H. M-band flexible wavelet transform and its application to the fault diagnosis of planetary gear transmission systems. Mech Syst Signal Pr 2019;134:106298. https://doi.org/10.1016/j.ymssp.2019.106298.
[12] Li Z, Yan X, Wang X, Peng Z. Detection of gear cracks in a complex gearbox of wind turbines using supervised bounded component analysis of vibration signals collected from multi-channel sensors. J Sound Vib 2016;371:406–33. https://doi.org/10.1016/j.jsv.2016.02.021.
[13] Glowacz A. Fault diagnosis of single-phase induction motor based on acoustic signals. Mech Syst Signal Pr 2019;117:20–7. https://doi.org/10.1016/j.ymssp.2018.07.044.
[14] Glowacz A. Acoustic based fault diagnosis of three-phase induction motor. Appl Acoust 2018;137:82–9. https://doi.org/10.1016/j.apacoust.2018.03.010.
[15] Glowacz A, Glowacz W, Glowacz Z, Kozik J. Early fault diagnosis of bearing and stator faults of the single-phase induction motor using acoustic signals. Measurement 2018;113:1–9. https://doi.org/10.1016/j.measurement.2017.08.036.
[16] Verma NK, Sevakula RK, Dixit S, Salour Al. Intelligent condition based monitoring using acoustic signals for air compressors. IEEE Trans Reliab 2016;65(1):291–309. https://doi.org/10.1109/TR.2015.2459684.
[17] Gunerkar RS, Jalan AK. Classification of ball bearing faults using vibro-acoustic sensor data fusion. Exp Techn 2019;43(5):635–43. https://doi.org/10.1007/s40799-019-00324-0.
[18] Mohanty S, Gupta KK, Raju KS. Hurst based vibro-acoustic feature extraction of bearing using EMD and VMD. Measurement 2017;117:200–20. https://doi.org/10.1016/j.measurement.2017.12.012.
[19] Li C, Sanchez RV, Zurita G, et al. Gearbox fault diagnosis based on deep random forest fusion of acoustic and vibration signals. Mech Syst Signal Pr 2016;76:283–93. https://doi.org/10.1016/j.ymssp.2016.02.007.
[20] Huang NE, Shen Z, Long SR, Wu MC, Shih HH, Zheng Q, et al. The empirical mode decomposition and the Hilbert spectrum for nonlinear and non-stationary time series analysis. Proc Roy Soc A Math Phys Eng Sci 1998;454(1971):903–95. https://doi.org/10.1098/rspa.1998.0193.
[21] Zhang X, Liu Z, Miao Q, Wang L. An optimized time varying filtering based empirical mode decomposition method with grey wolf optimizer for machinery fault diagnosis. J Sound Vib 2018;418:55–78. https://doi.org/10.1016/j.jsv.2017.12.028.
[22] Han D, Zhao N, Shi P. Gear fault feature extraction and diagnosis method under different load excitation based on EMD, PSO-SVM and fractal box dimension. J Mech Sci Technol 2019;33(2):487–94. https://doi.org/10.1007/s12206-019-0101-z.

[23] Niu Y, Fei J, Li Y, Wu D. A novel fault diagnosis method based on EMD, cyclostationary, SK and TPTSR. J Mech Sci Technol 2020;34(5):1925–35. https://doi.org/10.1007/s12206-020-0414-y.
[24] Wu ZH, Huang NE. Ensemble empirical mode decomposition:a noise-assisted data analysis method. Adv Adapt Data Anal 2009;1(1):1–41. https://doi.org/10.1142/S1793536909000047.
[25] Wang Y-H, Yeh C-H, Young H-W, Hu K, Lo M-T. On the computational complexity of the empirical mode decomposition algorithm. Phys A-Stat Mech Appl 2014;400:159–67. https://doi.org/10.1016/j.physa:2014.01.020.
[26] Yeh JR, Shieh JS, Huang NE. Complementary ensemble empirical mode decomposition: a novel noise enhanced data analysis method. Adv Adapt Data Anal 2010;2(2):135–56. https://doi.org/10.1142/S1793536910000422.
[27] Colominas MA, Schlotthauer G, Torres ME. Improved complete ensemble EMD: a suitable tool for biomedical signal processing. Biomed Signal Proces 2014;14:19–29. https://doi.org/10.1016/j.bspc.2014.06.009.
[28] Gilles J. Empirical wavelet transform. IEEE Trans Signal Proces 2013;61 (16):3999–4010. https://doi.org/10.1109/TSP.7810.1109/TSP.2013.2265222.
[29] Hu Y, Li F, Li H, Liu C. An enhanced empirical wavelet transform for noisy and non-stationary signal processing. Digit Signal Process 2017;60:220–9. https://doi.org/10.1016/j.dsp.2016.09.012.
[30] Dragomiretskiy K, Zosso D. Variational mode decomposition. IEEE Trans Signal Proces 2014;62(3):531–44. https://doi.org/10.1109/TSP.2013.2288675.
[31] Liu H, Mi XW, Li YF. Smart multi-step deep learning model for wind speed forecasting based on variational mode decomposition, singular spectrum analysis, LSTM network and ELM. Energ Convers Manage 2018;159:54–64. https://doi.org/10.1016/j.enconman.2018.01.010.
[32] Satija U, Trivedi N, Biswal G, Ramkumar B. Specific emitter identification based on variational mode decomposition and spectral features in single hop and relaying scenarios. IEEE Trans Inf Foren Sec 2019;14(3):581–91. https://doi.org/10.1109/TIFS.2018.2855665.
[33] Miao Y, Zhao M, Lin J. Identification of mechanical compound-fault based on the improved parameter-adaptive variational mode decomposition. ISA T 2018;84:82–95. https://doi.org/10.1016/j.isatra.2018.10.008.
[34] Jiang X, Wang J, Shi J, Shen C, Huang W, Zhu Z. A coarse-to-fine decomposing strategy of VMD for extraction of weak repetitive transients in fault diagnosis of rotating machines. Mech Syst Signal Pr 2019;116:668–92. https://doi.org/10.1016/j.ymssp.2018.07.014.
[35] Singh P, Joshi SD, Patney RK, Saha K. The Fourier Decomposition Method for nonlinear and nonstationary time series analysis. Proc Math Phys Eng 2017;473(2199):20160871. https://doi.org/10.1098/rspa.2016.0871.
[36] Elbi MD, Kizilkaya A. Multicomponent signal analysis: interwoven Fourier decomposition method. Digit Signal Process 2020;104:1–25. https://doi.org/10.1016/j.dsp.2020.102771.
[37] Fatimah B, Singh P, Singhal A, Pachori RB. Detection of apnea events from ECG segments using Fourier Decomposition Method. Biomed Signal Proces 2020;61:102005. https://doi.org/10.1016/j.bspc.2020.102005.
[38] Deng M, Deng A, Zhu J, Zhai Y, Sun W, Chen Q, et al. Bandwidth Fourier decomposition and its application in incipient fault identification of rolling bearings. Meas Sci Technol 2020;31(1):015012. https://doi.org/10.1088/1361-6501/ab4069.
[39] Wang J, Du G, Zhu Z, Shen C, He Q. Fault diagnosis of rotating machines based on the EMD manifold. Mech Syst Signal Pr 2020;135:106443. https://doi.org/10.1016/j.ymssp.2019.106443.
[40] Zou J, Bui K-T, Xiao Y, Doan CV. Dam deformation analysis based on BPNN merging models. Geo-Spatial Inf Sci 2018;21(2):149–57. https://doi.org/10.1080/10095020.2017.1386848.
[41] Deng W, Yao R, Zhao H, Yang X, Li G. A novel intelligent diagnosis method using optimal LS-SVM with improved PSO algorithm. Soft Comput 2019;23 (7):2445–62. https://doi.org/10.1007/s00500-017-2940-9.
[42] Inaba FK, Teatini Salles EO, Perron S, Caporossi G. DGR-ELM–distributed generalized regularized ELM for classification. Neurocomputing 2018;275:1522–30. https://doi.org/10.1016/j.neucom.2017.09.090.
[43] Wang Y, Xia ST, Tang Q, et al. A novel consistent random forest framework: Bernoulli random forests. IEEE Trans Neur Net Lear 2018;29(8):3510–23. https://doi.org/10.1109/TNNLS.2017.2729778.